Desalination and Water Treatment
www.deswater.com

doi: 10.5004/dwt.2021.27542

240 (2021) 2–13
November

Characterization of ion transfer and modeling of fouling in nanofiltration and reverse osmosis membranes

Hajar Zeggar[a], Jamal Touir[a], Soufian El-Ghzizel[a], Fatima Elazhar[a,b], Mustapha Tahaikt[a], Driss Dhiba[c], Azzedine Elmidaoui[a], Mohamed Taky[a,c,*]

[a]*Laboratory of Advanced Materials and Process Engineering, Faculty of Sciences, BP 1246, Kenitra, Morocco, emails: mohamed.taky@uit.ac.ma (M. Taky), zeggar.hajar@uit.ac.ma (H. Zeggar), jamal.touir@uit.ac.ma (J. Touir), soufian.el-ghzizel@uit.ac.ma (S. El-Ghzizel), fatima.elazhar@uit.ac.ma (F. Elazhar), mustapha.tahaikt@uit.ac.ma (M. Tahaikt), elmidaoui@uit.ac.ma (A. Elmidaoui)*
[b]*National Higher School of Chemistry (NHSC), Ibn Tofail University, Kenitra, Morocco*
[c]*International Water Research Institute, Mohammed VI Polytechnic University, Lot 660, Hay Moulay Rachid Ben Guerir, 43150 – Morocco, email: Driss.DHIBA@um6p.ma*

Received 24 May 2021; Accepted 21 June 2021

ABSTRACT

The first goal of this study is to provide a better understanding of the transfer mechanisms involved by nitrate, fluoride, chloride, and sulfate ions contained in nitrated brackish water. This part of the study is done by Spiegler-Kedem-Katchalsky (SKK) model that relates permeate flux to the rejection of the four anions by using a polyamide NF90 and BW30 membranes and leads to distinguish diffusion and convection phenomena. Secondly, the transport parameters determined using the SKK model (reflection coefficient σ and solute permeability P_s) are used in the steric hindrance pore (SHP) model to calculate the structural characteristics of the NF90 membrane. The results show that the permeabilities of ions in nanofiltration (NF) membrane are greater than that of reverse osmosis (RO) and, reflection coefficients (σ) are almost similar for both membranes. For the transfer process, the mechanism is convective and diffusional for the NF membrane, whereas for the RO membrane it is diffusional. The estimated average of r_p and $A_k/\Delta x$ for NF membrane are r_p = 0.16 nm and $\Delta x/A_k = 25.50 \times 10^{-7}$ m. Thirdly, this study is completed by a fouling investigation which is based on two experiments carried out separately. The first one is performed by studying the permeate flux decline vs. time. Based on the insight gained from these experiments, Hermia model is applied to determine exactly the type of fouling phenomenon. The second experiment for fouling investigation is based on the determination of different pure water permeability. The experimental data is applied to the resistance in series model to calculate the total resistance (R_t) related to both membranes, NF90 and BW30. The results of both fouling models obtained complemented each other and reveal the problems caused by the accumulation of deposits on the membrane surface. The results indicate that RO membrane is severely fouled than the NF membrane and, the fouling mode responsible for permeate flux decline for both membranes is the cake fouling.

Keywords: Modeling; Transfer mechanisms; Fouling; Spiegler–Kedem–Katchalsky; Steric hindrance pore model; Hermia model; Resistance in series model

* Corresponding author.

Presented at the Second International Symposium on Nanomaterials and Membrane Science for Water, Energy and Environment (SNMS-2021), June 1–2, 2022, Tangier, Morocco

1. Introduction

Nanofiltration (NF) and reverse osmosis (RO) are membrane processes widely used for nitrate removal and groundwater desalination thanks to their high efficiency and energy saving compared to conventional techniques [1–3]. Rejection and permeability in NF and RO membranes depend on the properties of the applied membrane (the number of pores, their form, and surface roughness) and the initial composition of the feed solution. The separation mechanisms in the NF membrane involve both steric and electrostatic partitioning effects between the membrane and solutions. Indeed, NF membranes retain molecules with a larger molecular weight than the molecular weight cut-off, which is a consequence of the steric exclusion effect whereby molecules larger than the membrane's pore size are rejected by the membrane. So, because of electrostatic interactions of ions with the charged surface of the membrane, NF membranes exhibit high retention of polyvalent ions compared to monovalent ions. For RO membranes, the transfer is governed by the solute-membrane interactions which are the consequence of the physical and chemical structures of these two entities [4–7].

Several studies have shown that NF membrane proves, in some applications, its competition to RO membrane, certainly allowing lower rejections but having the advantage of using lower transmembrane pressures (TMP) and higher solvent fluxes than those used in RO [8–12]. Despite the existence of several studies comparing NF and RO membranes in the treatment of water contaminated by nitrates and brackish groundwater desalination, these studies focus on the reduction of the nitrates in water without taking into account the transfer mechanisms of ions involved [13–15] or, they concentrate only on the fouling study [16–18]. To our knowledge, there are no studies that address both, the transfer mechanisms of ions and the fouling phenomenon of NF and RO membranes to treat nitrated effluent. In addition, according to literature research, the modeling of fouling applied on nitrated groundwater is a subject that is not widely addressed, on the contrary for wastewater treatment, this axis is widely studied and examined [19,20].

In order to understand and predict the transfer mechanisms of NF and RO membranes, it is necessary to dispose of reliable modeling tools linking the characteristics of the membrane to their transfer and fouling properties with respect to the effluent to be treated. Several models are proposed in the literature to describe the transfer mechanisms in NF and RO membranes [21–24]. Each model has been developed with specific conditions; they are based on diffusion, adsorption, ion-exchange, ion coupling, concentration polarization, or other mass transfer mechanisms. Membrane fouling, which is the most critical and common problem in membrane processes, refers to the phenomenon that suspended colloidal particles or dissolved macromolecules which are deposited on the membrane surface or adsorbed in the membrane pores in the process of membrane separation, resulting in the reduction or blockage of the membrane pores and decrease of membrane flux [25–27]. This phenomenon reduces the productivity of the membrane in terms of rejection and flux, and therefore contributes to the increase of energy expenditure and washing frequency, and presumably to the reduction of lifetime of membranes. The fouling phenomenon and its associated mechanisms of NF and RO membranes are generally investigated by using the Hermia empirical and the resistance-in-series models [28,29]

The first objective of this study is to analyze and predict the nitrate, fluoride, chloride, and sulfate anions rejection and understand the transfer mechanisms involved in two commercial membranes: NF90 and BW30 supplied by Dow Filmtec. Spiegler–Kedem–Katchalsky (SKK) model is used to predict reflection coefficient and solute permeability parameters. In addition, the steric hindrance pore (SHP) model is applied to calculate the structural characteristics of the NF membrane. The second objective focuses on the assessment and identification of the fouling phenomenon for NF90 and BW30 membranes in the treatment of nitrated brackish water. In order to identify the type of fouling, the permeate flux as a function of time is modeled by using the Hermia model. To quantify the resistance of the different fouling (internal and external), the resistance-in-series model is adopted. This model allows determining the total resistance of the membrane (R_t) after filtration from the value of the permeate flux measured on the basis of Darcy's law. This study is carried out on the real underground water of Bejaâd city which is located in the region of Chaouia-Ouardigha, Morocco.

2. Theory

2.1. Nanofiltration/reverse osmosis flux and rejection

The performance of the NF and RO membranes is measured in terms of rejection R and flux J_v which are defined by the following equations:

$$R = \left(1 - \frac{C_p}{C_f}\right) \times 100 \tag{1}$$

where C_p and C_f are the permeate and feed concentrations, respectively.

$$J_v = \frac{V}{t \times A} \tag{2}$$

where V is the volume of permeate collected in a given time interval t, and A is the membrane area.

2.2. Membrane mass transfer models

Generally, a mass transfer model aims at relating membrane performance (in terms of solute and solvent flux, and observed rejection) to operating conditions (driving pressure and concentration driving forces). This work is focused on two models:

2.2.1. Spiegler–Kedem–Katchalsky (SSK) model

The SKK model, based on irreversible thermodynamics was developed in 1966 [30]. In this model, the transport of solutes across a membrane is described using the principles of non-equilibrium thermodynamics where the

membrane is viewed as a black box. This approach makes it possible to characterize the membranes in terms of only the reflection coefficient σ and solute permeability P_s.

From this postulate, it is then possible to express the solvent flux J_v and the solute flux J_s as follows:

$$J_v = L_p\left(\Delta P - \sigma\Delta\pi\right) \tag{3}$$

$$J_s = P_s\left(C_m - C_p\right) + \left(1-\sigma\right)J_v C_m \tag{4}$$

where L_p is the membrane permeability to solvent, ΔP is the pressure, $\Delta\pi$ is the osmotic pressure due to the solute, σ is the reflection coefficient of the solute by the membrane, P_s is the permeability of the solute, C_m is the solute concentration at the membrane surface, C_p is the solute concentration in permeate.

The real rejection can be calculated by this theory as follows:

$$R_{\text{real}} = 1 - \frac{1-\sigma}{1-\sigma\exp\left[\left(\sigma-1\right)\left(\frac{J_v}{P_s}\right)\right]} \tag{5}$$

The reflection coefficient is a measure of the degree of separation of the membrane. s = 0 means no rejection and σ = 1 means rejection equals to 100%.

As seen from Eq. (4), the solute flux is the sum of the two terms one is diffusive the other is convective [31]. In general concentration difference on the membrane side and the permeate results in transport by diffusion, and the convection occurs because of the pressure gradient on both sides of the membrane. To assess the convective and diffusive contributions during solute mass transport in the membranes studied, the following expression was used [32,33]:

$$J_{\text{diff}} + J_v C_{\text{conv}} = C_p J_v \tag{6}$$

where ($J_{\text{diff}} = P_s\left(C_0 - C_p\right)$) and ($C_{\text{conv}} = (1-\sigma)\,C_m$).

Eq. (6) can be expressed as follows:

$$C_p = \frac{J_{\text{diff}}}{J_v} + C_{\text{conv}} \tag{7}$$

2.2.2. Steric hindrance pore model

To give a physical meaning and to interpret σ and P_s of the SKK model, several models have been used in the literature among these the SHP model. The SHP model developed by Nakao and Kimura in 1982 explains the interaction between the solute molecules and the membrane surface [34]. This model was used for the separation of aqueous solutions from a single organic solute by ultrafiltration membranes and subsequently was used successfully for NF membranes [35]. According to this model, σ and P_s are given as:

$$\sigma = 1 - S_F\left\{1 + \left(\frac{16}{9}\right)q^2\right\} \tag{8}$$

$$P_s = DS_D\left(\frac{A_k}{\Delta x}\right) \tag{9}$$

where:

$$S_D = \left(1-q\right)^2 \tag{10}$$

$$S_F = 2\left(1-q\right)^2 - \left(1-q\right)^4 \tag{11}$$

and

$$q = \frac{r_s}{r_p} \tag{12}$$

S_D and S_F are the averaged distribution coefficients related to the steric effect of the solute in conversion and diffusion conditions, respectively. D is the diffusivity; q is defined as the ratio of solute radius r_s to pore radius r_p; $A_k/\Delta x$ is the ratio of membrane porosity to membrane thickness. The Stokes radius used for calculations are calculated by the Stokes-Einstein formula Eq. (13), and presented in Table 1.

$$D = \frac{K_b T}{6\pi\mu r_s} \tag{13}$$

K_b is the Boltzmann constant, K_b = 1.38 × 10^{-23} J K^{-1}; T is the temperature, K; μ is the water viscosity at absolute temperature T, μ = 1.005 × 10^{-3} Pa.s; D is the diffusivity, $m^2.s^{-1}$

In an infinitely dilute solution, there are several methods for the prediction of the diffusion coefficient D. In this study, the Petr Vanýsek method was adopted [36].

On the other hand, another structural property which can influence the permeability is the porosity of the membrane. The structural parameter, $A_k/\Delta x$ can also be determined using the SHP model. L_p is expressed by Hagen-poiseuille in the SHP model and defined as:

$$L_p = \frac{r_p^2\left(\frac{A_k}{\Delta x}\right)}{8\mu} \tag{14}$$

2.3. Modeling fouling

To accurately predict fouling in the membranes studied, mathematical fouling models are used. The Hermia model is one of the most complete fouling prediction models and contains four different fouling mechanisms,

Table 1
Stokes radius of major anions used for calculations

Anions	Stokes radius (nm)
NO_3^-	0.114
Cl^-	0.121
F^-	0.146
SO_4^{2-}	0.231

Table 2
Filtration laws established by Hermia (1982)

Filtration laws	Cake formation	Intermediate blocking	Standard blocking	Complete blocking
Flux expression	$J_p = \frac{J_0}{\left(2K_{cf}J_0^2 t+1\right)^{\frac{1}{2}}}$ (15)	$J_p = \frac{J_0}{\left(K_{ib}J_0 t+1\right)}$ (16)	$J_p = \frac{4J_0}{\left(K_{sb}J_0^{\frac{1}{2}} t+2\right)^2}$ (17)	$J_p = J_0\exp\left(-K_{cb}t\right)$ (18)

namely full blockage, intermediate blockage, standard blockage, and filter cake formation. In addition, the series resistance model derived from classical filtration theory is used to calculate the hydraulic resistance caused by the fouling on the membrane.

2.3.1. Hermia model

Hermia proposed models which separately describe the different modes of membrane fouling (29). These models made for frontal filtration were modified by Field et al. [37,38] who inserted a deposit erosion parameter to take into account of the effect of the shear created by the recirculation of the permeate in the case of tangential filtration [39]. Hermia proposed four fouling models allowing a better understanding of the fouling mechanisms that occur on the surface of the membrane and/or inside its pores. Table 2 gives the filtration laws established by Hermia.

2.3.2. Resistance-in-series model

When filtering real water, a decrease in the permeability of the membrane is observed over time, due to the fouling phenomenon; this is induced by the increased resistance to filtration. Darcy's law can be changed by introducing series resistors. The overall hydraulic resistance (R_t) is defined as the sum of the resistance of the membrane (R_m), that due to the concentration polarization layer (R_c) and the additional resistance due to fouling (R_f) [40].

$$J_v = \frac{\text{PTM}}{\mu\left(R_m + R_c + R_f\right)} \tag{19}$$

with:

$$R_f = R_{rev} + R_{irrv} \tag{20}$$

The fouling resistance R_f is a combination of the resistance caused by reversible fouling R_{rev} and irreversible fouling R_{irrv}.

$$R_m = \frac{1}{\mu L_p^0} \tag{21}$$

$$R_t = \frac{1}{\mu L_p^1} \tag{22}$$

$$R_m + R_f = \frac{1}{\mu L_p^2} \tag{23}$$

$$R_m + R_{irrv} = \frac{1}{\mu L_p^3} \tag{24}$$

μ is the viscosity of pure water (Pa·s); L_p^i is the permeability to pure water of the membrane (m Pa^{-1} s^{-1}); L_p^0 is the permeability to pure water of the membrane before processing the raw water, L_p^1 is the permeability to pure water of the membrane after processing the raw water, L_p^2 is the permeability to pure water of the membrane after rinsing the membrane with water, L_p^3 is the permeability to pure water of the membrane after chemical cleaning of the membrane.

3. Materials and methods

3.1. NF and RO setup

The experiments were performed on an NF/RO pilot plant (E 3039) supplied by TIA Company (Technologies Industrielles Appliquées, France) shown in Fig. 1. The applied pressure over the membrane can be varied from 5 to 70 bar with manual valves. The pilot plant is equipped with two identical pressure vessels operating in series. Each pressure vessel contains one element. The pressure loss is about 2 bar corresponding to 1 bar of each pressure vessel. The two spiral wound modules are equipped with two commercial membranes of one type. Table 3 gives the characteristics of the membranes used.

3.2. Characteristics of the feed water

The analytical results of the feed water give the results shown in Table 4. This water is real slightly brackish water which is not in conformity with sanitary standards because of the high concentrations of nitrate (50 mg/L) [41].

3.3. Operating conditions/analysis

After the run, the membranes were cleaned with alkaline and acidic cleaning solutions according to the manufacturer's recommendations. Pure water permeability is determined by plotting flux j_v vs. TMP. The hydraulic properties of the studied membranes are analyzed by measuring water flux as a function of TMP. Samples of permeate were collected and water parameters were determined analytically following standard methods previously described in [42].

4. Results and discussion

4.1. Prediction of the permeability

Fig. 2 shows the dependency of TMP on flux through both membranes. The results indicate a linear relationship

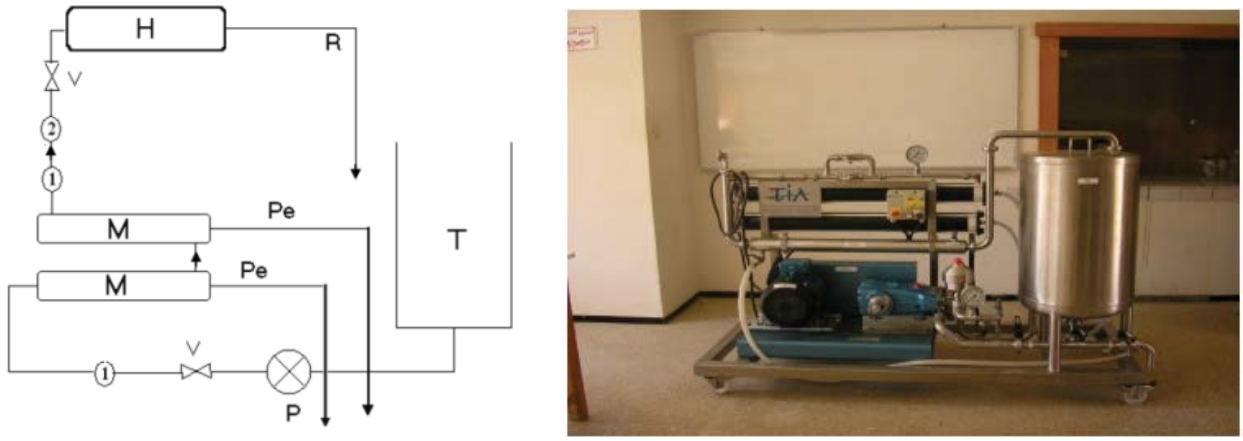

Fig. 1. Diagram and picture of the nanofiltration pilot plant. T: tank; P: feed pump; V: pressure regulation valves; M: NF/RO module; Pe: permeate recirculation; R: retentate recirculation; H: heat exchanger; 1: pressure sensor; 2: temperature sensor.

Table 3
Characteristics of the used membranes

Membrane	BW30 LE4040	NF90
Area (m²)	7.2	7.6
P_{max}(bar)	41	41
pH	2–11	3–10
Max. temp. (°C)	45	45
Materials	Polyamide	Polyamide
Cl_2 tolerance ppm	0.1	0.1

Table 4
Characteristics of the feed underground water

Parameters	Feed water
Conductivity (µs/cm)	1,330
NO_3^-(mg/L)	119
Cl^-(mg/L)	536
F^-(mg/L)	1.2
SO_4^{2-}(mg/L)	230
Hardness (F°)	30.66
Alkalinity (F°)	30

between the water flux and the TMP. This is explained by Eq. (3) because separation in NF/RO is a pressure-driven process. As the TMP increases, thereby increasing the driving force, this leads to an increase in the flux. High fluxes of NF membranes at low pressure confirmed that NF membranes can be used as in energy saving compared to RO membranes. The permeability of NF membrane is higher than RO membrane because NF membrane has a looser network of polymer compared to RO membrane. The permeability of the membranes tested does not vary significantly during the experiments, therefore the membranes can be considered stable during the experiments Table 5.

4.2. TMP effect on ion rejections

As shown in Fig. 3, rejections of sulfate and fluoride are almost similar for the two membranes. In contrast, for nitrate and chloride rejection, RO and NF membranes

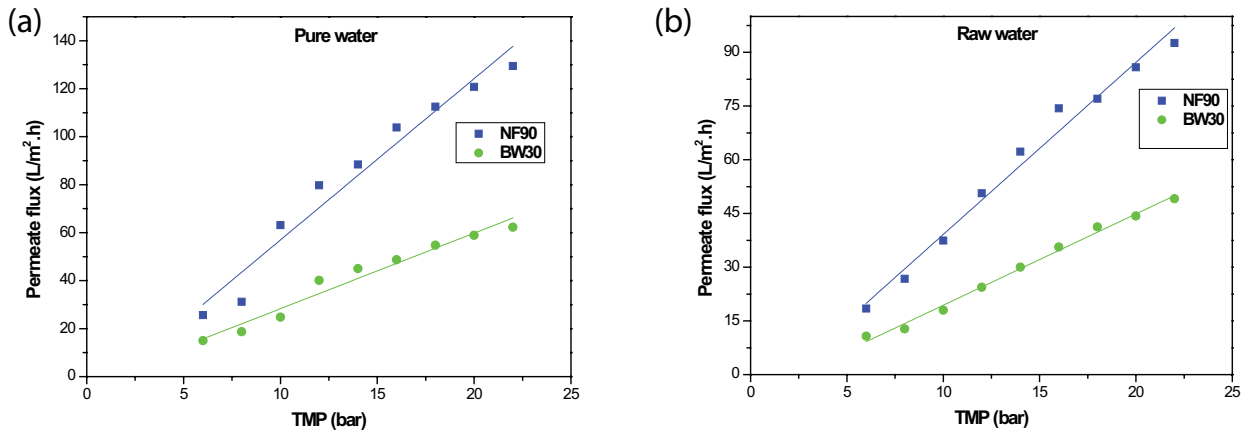

Fig. 2.(a) Pure water flux and (b) raw water flux vs. TMP.

Table 5
Permeability of membranes with different feed solutions

	NF90		BW30	
	Pure water	Raw water	Pure water	Raw water
Permeability (L m^{-2} h^{-1} bar^{-1})	6.72	4.80	3.15	2.54
Adj. R-square	95.53	98.13	95.81	99.19

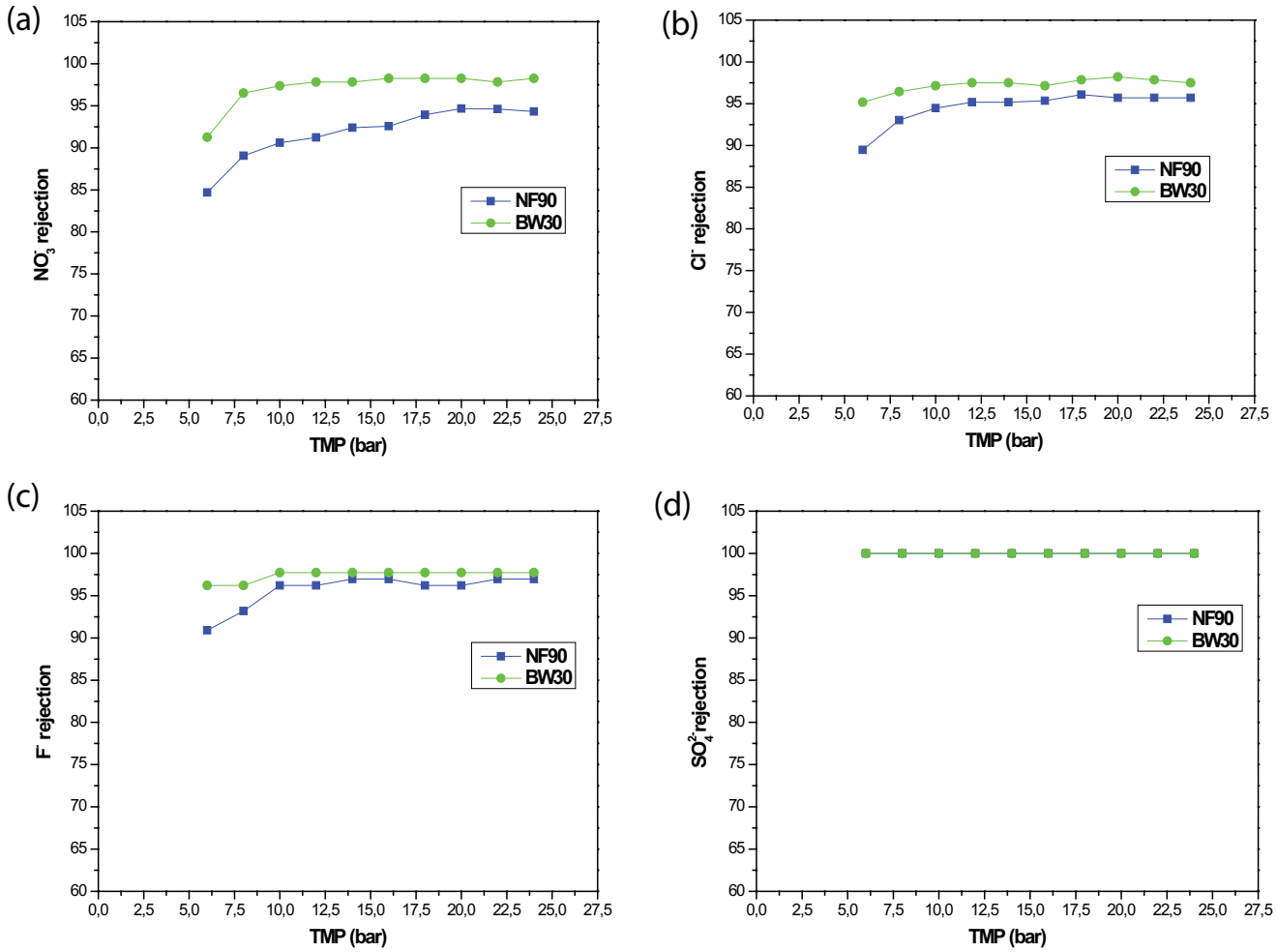

Fig. 3. Rejection of (a) nitrate, (b) chloride, (c) fluoride and (d) sulfate vs. TMP.

exhibit different values. The same figure shows that ion rejections increase as a function of TMP. The increase in TMP leads to an increase in solvent flux. In this case, the ion fluxes remain unchanged due to the rejection of ions by steric/charge interactions which leads to a dilution of the permeate. Therefore, a high rejection is observed for all the studied ions [43].

4.3. SKK model

Fig. 4 shows the variation of the experimental and modulated rejection using the SSK model for nitrate, chloride, fluoride, and sulfate as a function of permeate flux. The solute rejection increases with permeate flux for the four anions. This behavior is due to the preferential passage of water through the membrane. Through nonlinear fitting, the values of σ and P_s are obtained by using Eq. (5). The obtained results are presented in Table 6. These results show that RO membrane exhibits a higher nitrate rejection than NF ($\sigma_{RO} > \sigma_{NF}$). On the other hand, the permeability of nitrate ions in the NF membrane is greater than that of RO (P_s (NF) > P_s (RO)). Similar results are obtained for the other ions in terms of P_s, but for σ_{RO} and σ_{NF}, the results obtained are almost similar. Similar results were found for NF and RO by Tahaikt et al. [44] and Zouhri et al. [45]. The P_s values depend on the type of ions. Strongly

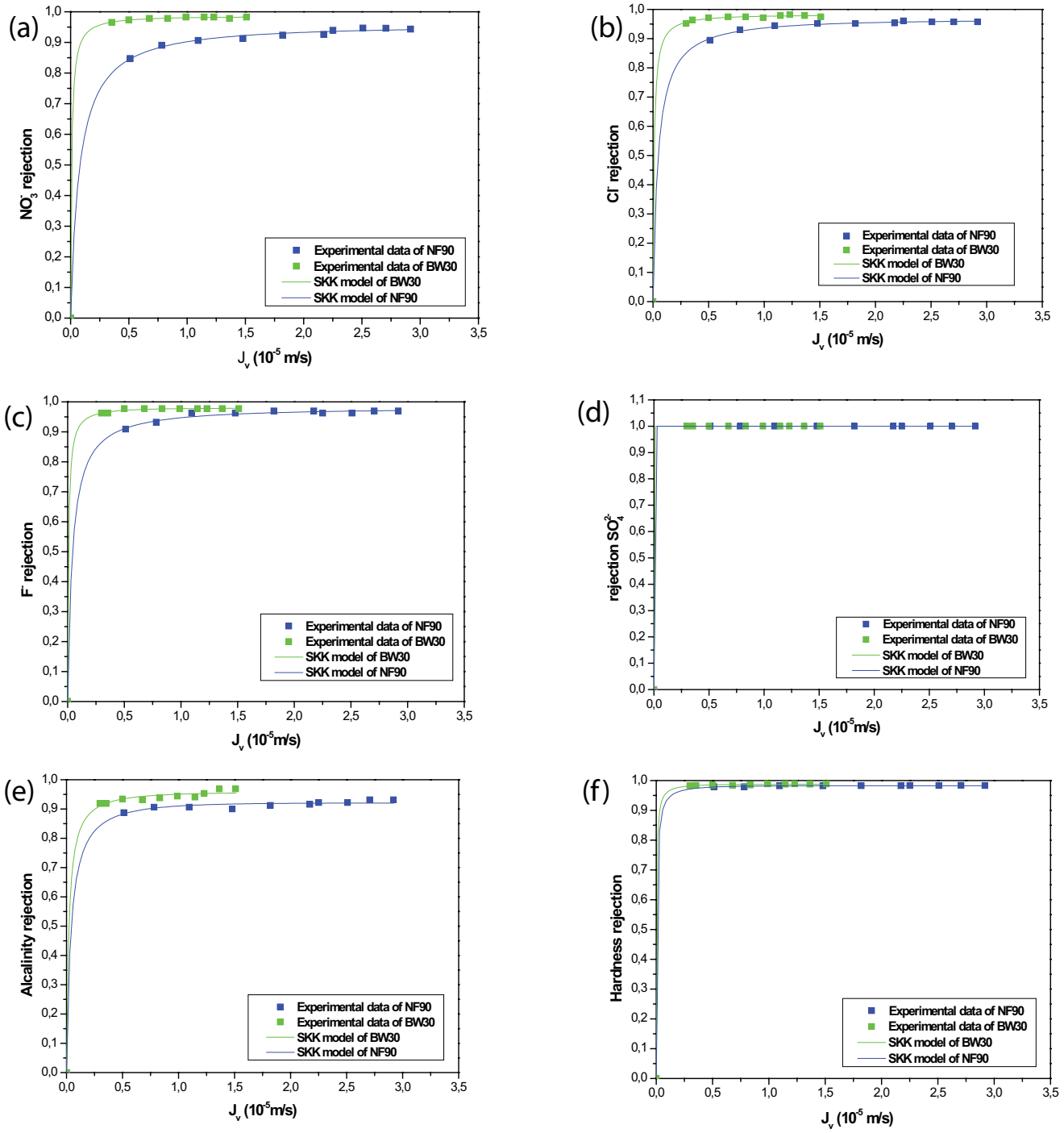

Fig. 4. Rejection for of (a) nitrate, (b) chloride, (c) fluoride and (d) sulfate, (e) alkalinity and (f) hardness vs. J_v.

solvated sulfate anions lead to lower P_s values compared to less solvated monovalent anions $P_s(SO_4^{2-}) < P_s(F^-) < P_s(Cl^-) < P_s(NO_3^-)$ [31]. For each ion, the σ-value depends on the order of the hydration energy. This parameter is higher for sulfate than other anions F^-, Cl^-, NO_3^-. From Fig. 4, it appears that the model obtained with the estimated parameters significantly explains the rejection behavior of both membranes. There is also a perfect fit between the theoretical model and the experimental results.

The obtained data allows distinguishing the diffusion and convection phenomena. According to the SKK model, both membranes have high reflection coefficients σ, a high reflection coefficient indicates that the convection transport is very low, and the predominance of diffusion contribution is reserved especially for RO membrane.

To confirm the mechanism of diffusive and convective transfer of ions in both membranes, the concentration in the permeate is plotted as a function of the $(1/J_v)$ in

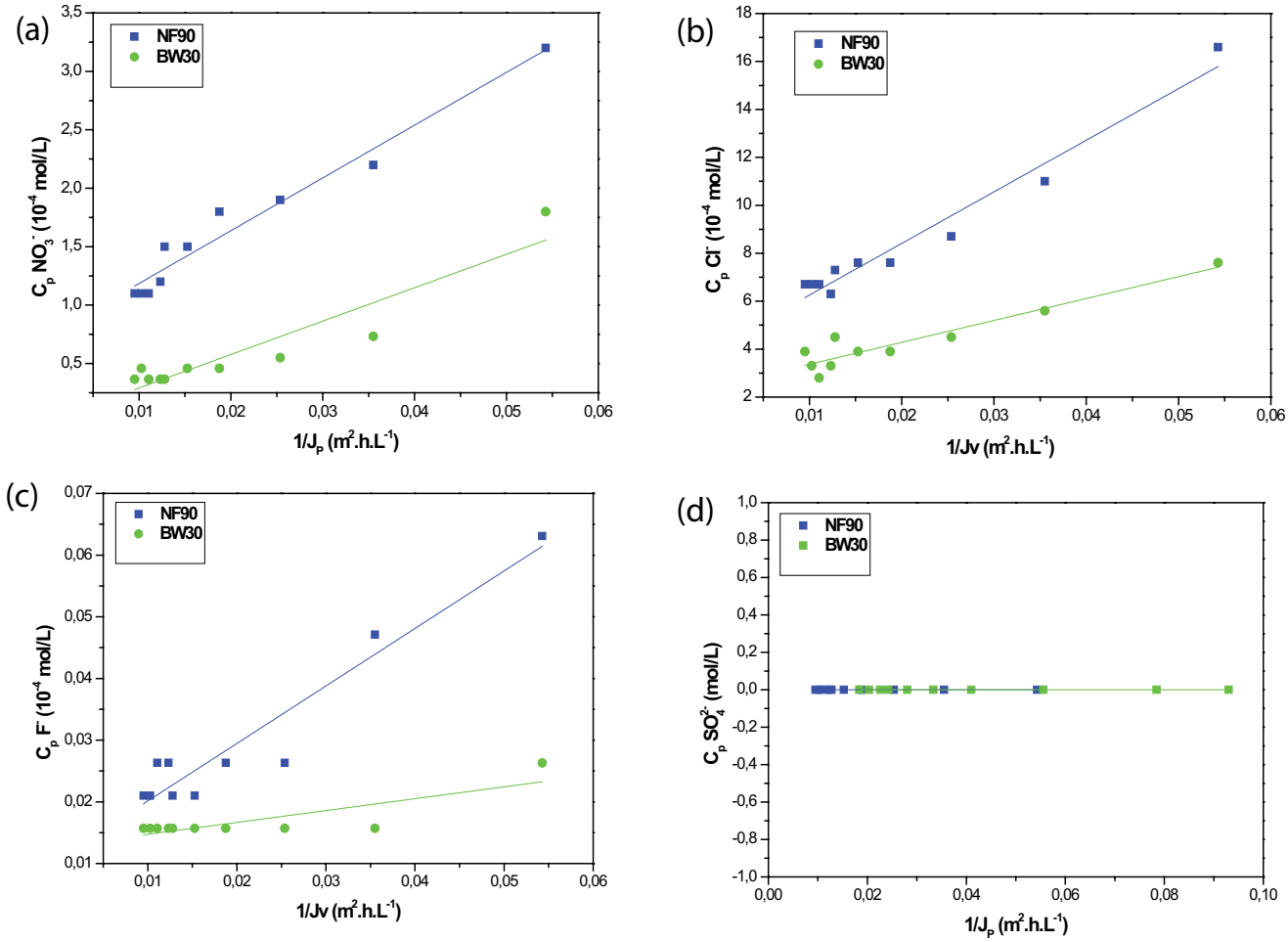

Fig. 5. Concentration of (a) nitrate, (b) chloride, (c) fluoride and (d) sulfate in the permeate vs. $1/J_v$

Table 6
Calculated P_s and s for tested membranes

Ions	Parameters P_s,σ and their R-square	NF90	BW30
NO_3^-	Permeability to solute P_s (m/s)	7.45×10^{-7}	8.92×10^{-8}
	Reflection coefficient σ	0.94904	0.98351
	Adj. R-Square	0.99	0.99
Cl^-	Permeability to solute P_s (m/s)	4.46×10^{-7}	1.00×10^{-7}
	Reflection coefficient σ	0.96339	0.97963
	Adj. R-square	0.99	0.99
F^-	Permeability to solute P_s (m/s)	4.18×10^{-7}	0.80×10^{-8}
	Reflection coefficient σ	0.97661	0.97887
	Adj. R-square	0.99	0.99
SO_4^{2-}	Permeability to solute P_s (m/s)	-1.26×10^{-10}	-5.33×10^{-11}
	Reflection coefficient σ	0.99794	0.99799
	Adj. R-square	1	1

Fig. 5. The intercept allows to know the concentration in the permeate due to convection C_{conv} and the slope allows to determine the flow of solute transported by diffusion J_{diff} Eq. (7). The C_{conv} and J_{diff} values obtained are presented in Table 7. According to these results, the C_{conv} of ions are low and the value obtained by NF membrane is greater than that RO membrane. The J_{diff} of ions are greater for NF than for RO. In RO membrane, since values of C_{Conv}

are very low, the transfer is governed by diffusion. For NF membrane, it appears that the transfer mechanism is more convective than for RO membrane. Based on the slope (J_{diff}) results, the characteristic of the pure diffusion phenomenon is important for NF. Overall, the NF transfer process is convective and diffusional, whereas for the RO it is diffusional. Calculated values of C_{conv} tend towards zero for both membranes. These results show that the properties of the mass transfer for NF membrane studied are close to those of the RO membranes. Finally, the two membranes studied involve convection and diffusion transfer mechanisms, both acting separately, but additively on the transfer, and with a low contribution of convection.

4.4. SHP model

NF differs from RO by its porous structure. Therefore, it is essential to determine the structural characteristics of this membrane, in order to appreciate the transfer mechanisms involved. Table 8 summarizes the values of q, r_p, and $A_k/\Delta x$ for the NF membrane by SHP model. q is calculated by Eqs. (11) and (14). r_p and $A_k/\Delta x$ are calculated respectively by Eqs. (12) and (14). The value of q for ions is close to 1 indicating the high rejection of these ions. The ratio $A_k/\Delta x$ increases with the increase in the Stokes radius of the ion. The estimated average of r_p and $A_k/\Delta x$ for NF membrane are r_p = 0.16 nm, $\Delta x/A_k$ = 25.50 × 10^{-7} m. Fatehizadeh et al. [43] investigated fluoride rejection by NF90 obtained r_p = 0.12 nm and $\Delta x/A_k$ = 4.784 × 10^{-4} m. The pore radius obtained by our study and that of Fatehizadeh et al. is significantly lower than that of the virgin membrane. This can be expressed by the fact that any kind of material deposited inside the pores results in the reduction of the pores radius. In another study conducted by Curatas-Uribe et al. [46], the authors found r_p = 0.41 nm for lactose rejection. The r_p calculated in this study (0.16 nm) is smaller than that found by these researchers (0.41 nm), r_p = 0.16 nm seems to be in line with the performance of NF90 and its structure which exhibiting small pore size and low porosity.

4.5. Membrane fouling study

Fig. 6 shows permeate flux vs. time for NF and RO membranes. According to this result, permeate flux decline for both membranes by 69% and 49% for NF and RO respectively for a (t = 3.9 × 10^3 s). Firstly, the permeate flux decreases rapidly due to concentration polarization, resulting in an accumulation of rejected solutes or particles in a mass transfer boundary layer to the membrane surface. The retained particles create a concentration gradient at the membrane surface which prevents the solvent from flowing through the membrane. This concentration polarization phenomenon is reversible and does not affect the intrinsic properties of the membrane. Then a slight decrease is observed until (t = 1.4 × 10^3 s). Finally, the flux becomes stationary due to the fouling phenomenon, which results in the deposition of particles on the membrane surface, or by adsorption of particles inside its porous structure. Unlike concentration polarization, fouling can cause an irreversible loss of membrane permeability.

Table 7
Calculated J_{diff} and C_{conv} of studied anions for NF90 and BW30 membranes

Ions	Parameters J_{diff}, C_{conv} and their R-square	NF90	BW30
NO_3^-	J_{diff} (L/h m²)	7.33	0.00452
	C_{conv} (mol/L)	7.33 × 10^{-5}	5.41 × 10^{-7}
	Adj. R-square	95.75	85.90
Cl^-	J_{diff} (L/h m²)	0.02153	0.00914
	C_{conv} (mol/L)	4.10225 × 10^{-4}	2.45455 × 10^{-4}
	Adj. R-square	95.96	88.19
F^-	J_{diff}(L/h m²)	9.32 × 10^{-5}	1.92 × 10^{-5}
	C_{conv} (mol/L)	1.08 × 10^{-6}	1.28 × 10^{-6}
	Adj. R-square	90.59	64.06
SO_4^{2-}	J_{diff} (L/h m²)	–	–
	C_{conv} (mol/L)	–	–
	Adj. R-square	–	–

Table 8
SHP parameters of NF90

Ions	q	r_p (nm)	$\Delta x/A_k$ (m)
NO_3^-	0.897	0.12	9.59 × 10^{-8}
Cl^-	0.914	0.13	1.12 × 10^{-7}
F^-	0.932	0.15	1.49 × 10^{-7}
SO_4^{2-}	0.98	0.23	3.52 × 10^{-7}

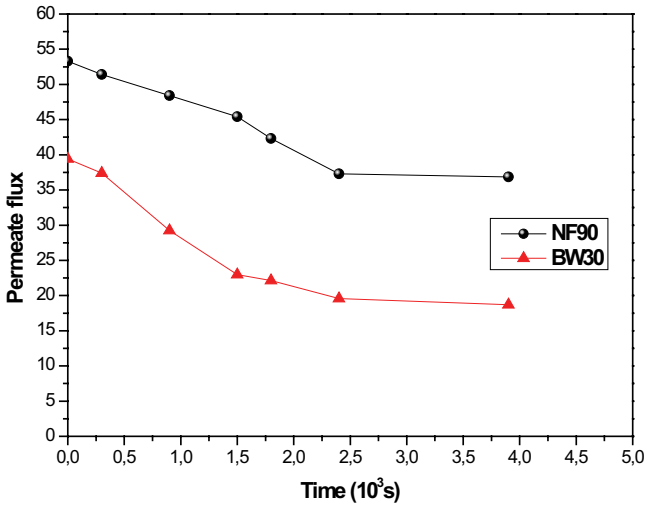

Fig. 6. Permeate flux vs. time for NF and RO membrane.

4.5.1. Hermia model

In order to determine the fouling mode responsible for permeate flux decline, the study is performed on the two membranes in semi-batch mode configuration. Then the expressions of the flux relating to the four fouling mechanisms of the Hermia model Eqs. (15)–(18) are considered. More precisely, we study the variation of the permeate

flux as a function of time, we set the value of the initial flux J_0 and we optimize the K_i parameters. Fig. 7 shows experimental and modeling data using the Hermia model for NF90 and BW30. K_i parameters obtained from modeling of fouling according to the Hermia model are collected in Table 9. For both membranes, analysis of the optimized values of K_i parameter reveals that K_{cf} values are higher than those of K_i. Also, the *R*-square of K_{cf} is the largest (exceeds 94%), which shows good accordance between the experimental and modeled results. This result indicates that the cake fouling mode is predominant. Calculate K_{cf} for BW30 membrane is higher than the value calculated for NF90 membrane. The value of K_{ib} is higher compared to the values of K_{sb} and K_{cb}; this finding means that foulants particles have larger diameters than the pores of the membrane. In this case, foulants particles superimpose on the membrane surface pores or form a cake on its surface. Thus, K_{ib} further promotes the cake formation; the foulants particles are more deposited in the pores, the cake layer thickness increases.

4.5.2. Resistance in series model

To complete the fouling study, resistance in series model is used to quantify the resistance of the various fouling and to determine the resistance responsible for flux decline. Table 10 shows the collected value of different types of resistance during NF90 and BW30 filtration. The membrane resistance R_m is higher for BW30 which is a RO membrane, since these membranes are considered dense. RO membrane presents some interstices that allow the passage of the solvent. So there are more obstacles for the solvent to cross RO membrane compared to partially porous NF membrane.

The concentration polarization resistance (R_c) and the fouling resistance (R_f) for the BW30 membrane is higher than that obtained in NF90 membrane which means that RO membrane is severely fouled than NF membrane. RO membrane is known for its high rejection of total dissolved solids (TDS) which generate a great concentration polarization on the membrane surface compared to NF membrane. In the fouling phenomenon, foulants particles in NF90 membrane are distributed between those which penetrate the pores and those which are deposited on the surface of the membrane are spread between those which enter the pores and those which are deposited on the surface. While for BW30, foulants particles deposed on the surface of the membrane, which causes faster and greater fouling.

From Table 10, the percentage of R_c from the share of total resistance is 17.83% and 11.51% for NF90 and BW30, respectively. At the same time, the percentage of R_f from the share of the total resistance is 10% for NF90 and 6.47% for

Table 9
Calculated K_i values for NF90 and BW30 membranes

	NF90		BW30	
	K_i	*R*-square	K_i	*R*-square
K_{cf} (s m^{-2})	71.29×10^{4}	94.37	4.420×10^{6}	95.91
K_{sb} (s$^{-1/2}$)	33.04×10^{-3}	93.46	99.22×10^{-3}	93.62
K_{ib} (m^{-1})	9.06	94.12	35.40	95.56
K_{cb} (s^{-1})	1.13×10^{-4}	92.34	2.74×10^{-4}	89.65

Table 10
Calculated resistances values for NF90 and BW30

Resistance (m^{-1})	NF90	BW30
R_t	7.40×10^{13}	1.39×10^{14}
R_m	5.34×10^{13}	1.14×10^{14}
R_c	1.32×10^{13}	0.16×10^{14}
R_f	0.74×10^{13}	0.09×10^{14}
R_{rev}	0.68×10^{13}	0.06×10^{14}
R_{irrev}	0.06×10^{13}	0.03×10^{14}
R_m/R_t	72.16%	82.01%
R_c/R_t	17.83%	11.51%
R_f/R_t	10%	6.47%

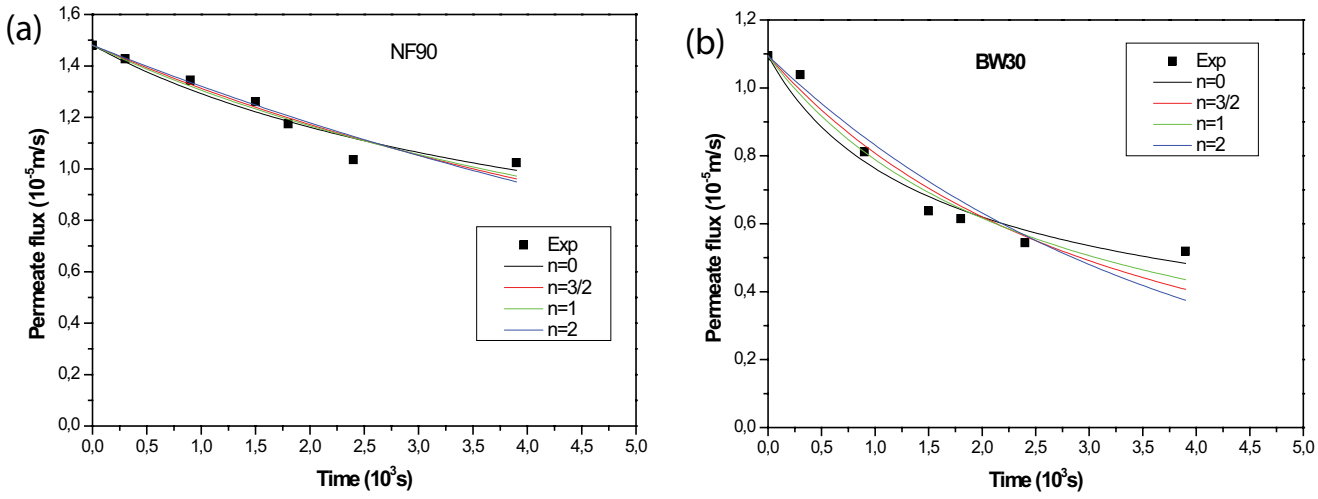

Fig. 7. Experimental data fitting with Hermia model for (a) NF90 and (b) BW30 membranes.

BW30. These results indicate that R_c has a greater share of the total resistance than R_f. This greater polarization concentration resistance could result from the increased cake of the fouling layer. In addition, the percentages of the two resistances observed are greater for NF membrane than that calculated for RO membrane, this could be associated with the higher permeate flux of NF membrane in comparison with RO membrane.

Finally, the calculated resistances show also that predominately fraction of fouling in both NF90 and BW30 membranes is reversible and only a small fraction will require chemical cleaning to be removed.

5. Conclusion

SKK model allows to predict ions rejection by calculating the permeability of solutes and the reflection coefficient. Also, this model provides information on the convective and diffusion transfer mechanisms of ions in the membrane. Rejection of the studied ions by NF90 and BW30 membranes in the treatment of water contaminated by nitrate is almost similar. The SKK model shows a good agreement between the theoretical fit model and the experimental data. This study shows that σ and P_s depend on the nature of anion. In addition, the transport mechanism in NF90 is convective and diffusional, whereas, for BW30, the transport is mainly diffusive. In parallel, the most drawbacks of this model are attributed to the lack of explanation of the nature of the membrane structure and its ignorance of the impact of concentration polarization which is the seat of solute-solvent interactions.

The SHP model provides additional information about membrane characteristics (pore radius, porosity, and thickness) which contributes to understanding the transport mechanisms involved in the NF process, but this model is limited by the fact that it only takes into consideration the steric effect of the membrane but without taking into account the electrostatic interactions between the solute and the membrane surface. The membrane characterization study shows that the estimated average of r_p and $A_k/\Delta x$ of the NF membrane are r_p = 0.16 nm and $\Delta x/A_k = 25.50 \times 10^{-7}$ m.

The fouling modeling is evaluated using the Hermia and the resistance-in-series models. The Hermia model shows a good agreement between the experimental and model results. In addition, it provides a good explication of the fouling type involved during the membrane filtration experiment. It reveals that the cake fouling mode is predominant for both membranes. Also, the fouling study is completed by using the resistance-in-series model. The results show that RO membrane is severely fouled than NF membrane and the predominately fraction of fouling in NF and RO membranes is reversible and only a small fraction will require a chemical cleaning to be removed. These two models are complementary for a good understanding of fouling.

References

[1] S. El-Ghzizel, H. Jalté, B. Bachiri, A. Zdeg, F. Tiyal, M. Hafsi, M. Taky, A. Elmidaoui, Demineralization of underground water by a nanofiltration plant coupled with a photovoltaic and wind energy system, Desal. Water Treat., 130 (2018) 28–36.

[2] F. El Azhar, M. Tahaikt, N. Zouhri, A. Zdeg, M. Hafsi, K. Tahri, H. Bari, M. Taky, M. Elamrani, A. Elmidaoui, Remineralization of reverse osmosis (RO)-desalted water for a Moroccan desalination plant: optimization and cost evaluation of the lime saturator post, Desalination, 300 (2012) 46–50.

[3] F. Elazhar, M. Elazhar, M. Hafsi, M. Taky, A. Elmidaoui, Desalination of brackish water using low pressure nanofiltration membranes: comparison and simulation. J. Chem. Pharm. Res., 10 (2018) 119–125.

[4] M. Pontié, H. Dach, J. Leparc, M. Hafsi, A. Lhassani, Novel approach combining physico-chemical characterizations and mass transfer modelling of nanofiltration and low pressure reverse osmosis membranes for brackish water desalination intensification, Desalination, 221 (2008) 174–191.

[5] V. Geraldes, M.D. Afonso, Generalized mass-transfer correction factor for nanofiltration and reverse osmosis, AIChE J., 52 (2006) 3353–3362.

[6] P. Dechadilok, W.M. Deen, Hindrance factors for diffusion and convection in pores, Ind. Eng. Chem. Res., 45 (2006) 6953–6959.

[7] R. Bonner, C. Germishuizen, S. Franzsen, Prediction of nanofiltration rejection performance in brackish water reverse osmosis brine treatment processes, J. Water Process Eng., 32 (2019) 100900. doi: 10.1016/j.jwpe.2019.100900

[8] F. Elazhar, J. Touir, M. Elazhar, S. Belhamidi, N. El Harrak, A. Zdeg, M. Hafsi, Z. Amor, M. Taky, A. Elmidaoui, Techno-economic comparison of reverse osmosis and nanofiltration in desalination of a Moroccan brackish groundwater, Desal. Water Treat., 55 (2015) 2471–2477.

[9] H. Dach, Comparison of Nanofiltration and Reverse Osmosis Processes for a Selective Desalination of Brackish Water Feeds, Engineering Sciences [Physics]. Université d'Angers, 2008. Available at: https://tel.archives-ouvertes.fr/tel-00433513 (accessed February 17, 2020).

[10] N. El Harrak, F. Elazhar, S. Belhamidi, M. Elazhar, J. Touir, A. Elmidaoui, Comparaison des performances des deux procédés membranaires: la Nanofiltration et de l'Osmose inverse dans le Dessalement des eaux saumâtres (Performances comparison of two membranes processes: nanofiltration and reverse osmosis in brackish water desalination), J. Mater. Environ. Sci., 6 (2015) 383–390.

[11] M. Tahaikt, A. Ait Haddou, R. El Habbani, Z. Amor, F. Elhannouni, M. Taky, M. Kharif, A. Boughriba, M. Hafsi, A. Elmidaoui, Comparison of the performances of three commercial membranes in fluoride removal by nanofiltration. Continuous operations, Desalination, 225 (2008) 209–219.

[12] G. Vaseghi, A. Ghassemi, J. Loya, Characterization of reverse osmosis and nanofiltration membranes: effects of operating conditions and specific ion rejection, Desal. Water Treat., 57 (2016) 23461–23472.

[13] J. Cuhorka, E. Wallace, P. Mikulášek, Removal of micropollutants from water by commercially available nanofiltration membranes, Sci. Total Environ., 720 (2020) 137474. doi: 10.1016/j.scitotenv.2020.137474

[14] F. Labarca, R. Bórquez, Comparative study of nanofiltration and ion exchange for nitrate reduction in the presence of chloride and iron in groundwater, Sci. Total Environ., 723 (2020) 137809. doi: 10.1016/j.scitotenv.2020.137809

[15] R. Epsztein, O. Nir, O. Lahav, M. Green, Selective nitrate removal from groundwater using a hybrid nanofiltration-reverse osmosis filtration scheme, Chem. Eng. J., 279 (2015) 372–378.

[16] D. Lin, L. Bai, D. Xu, H. Wang, H. Zhang, G. Li, H. Liang, Nanofiltration scaling influenced by coexisting pollutants considering the interaction between ferric coagulant and natural organic macromolecules, Chem. Eng. J., 413 (2021) 127403. doi: 10.1016/j.cej.2020.127403

[17] E.A. Roehl, D.A. Ladner, R.C. Daamen, J.B. Cook, J. Safarik, D.W. Phipps, P. Xie, Modeling fouling in a large RO system with artificial neural networks, J. Membr. Sci., 552 (2018) 95–106.

[18] S. El-ghzizel, H. Jalte, H. Zeggar, M. Zait, S. Belhamidi, F. Tiyal, M. Hafsi, M. Taky, A. Elmidaoui, Autopsy of nanofiltration membrane of a decentralized demineralization plant, Membr. Water Treat., 10 (2019) 277–286.

[19] M. Mehdi Amin, E. Taheri, A. Fatehizadeh, M. Rezakazemi, T.M. Aminabhavi, Anaerobic membrane bioreactor for the production of bioH2: electron flow, fouling modeling and kinetic study, Chem. Eng. J., (2021) 130716. doi: 10.1016/j.cej.2021.130716
[20] S.J. Im, N.D. Viet, A. Jang, Real-time monitoring of forward osmosis membrane fouling in wastewater reuse process performed with a deep learning model, Chemosphere, 275 (2021) 130047. doi: 10.1016/j.chemosphere.2021.130047
[21] A. Ghorbani, B. Bayati, E. Drioli, F. Macedonio, T. Kikhavani, M. Frappa, Modeling of nanofiltration process using DSPM-DE model for purification of amine solution, Membranes (Basel), 11 (2021) 230, doi: 10.3390/membranes11040230.
[22] S.M.J. Zaidi, F. Fadhillah, Z. Khan, A.F. Ismail, Salt and water transport in reverse osmosis thin film composite seawater desalination membranes, Desalination, 368 (2015) 202–213.
[23] L. Pérez, I. Escudero, M.J. Arcos-Martínez, J.M. Benito, Application of the solution-diffusion-film model for the transfer of electrolytes and uncharged compounds in a nanofiltration membrane, J. Ind. Eng. Chem., 47 (2017) 368–374.
[24] A. Yaroshchuk, M.L. Bruening, E. Zholkovskiy, Modelling nanofiltration of electrolyte solutions, Adv. Colloid Interface Sci., 268 (2019) 39–63.
[25] X. Meng, D. Luosang, S. Meng, R. Wang, W. Fan, D. Liang, X. Li, Q. Zhao, L. Yang, The structural and functional properties of polysaccharide foulants in membrane fouling, Chemosphere, 268 (2021) 129364. doi: 10.1016/j.chemosphere.2020.129364
[26] S.K. Mah, C.K. Chuah, W.P. Cathie Lee, S.P. Chai, Ultrafiltration of palm oil-oleic acid-glycerin solutions: fouling mechanism identification, fouling mechanism analysis and membrane characterizations, Sep. Purif. Technol., 98 (2012) 419–431.
[27] M.J. Corbatón-Báguena, M.C. Vincent-Vela, J.M. Gozálvez-Zafrilla, S. Álvarez-Blanco, J. Lora-García, D. Catalán-Martínez, Comparison between artificial neural networks and Hermia's models to assess ultrafiltration performance, Sep. Purif. Technol., 170 (2016) 434–444.
[28] E.E. Chang, S.Y. Yang, C.P. Huang, C.H. Liang, P.C. Chiang, Assessing the fouling mechanisms of high-pressure nanofiltration membrane using the modified Hermia model and the resistance-in-series model, Sep. Purif. Technol., 79 (2011) 329–336.
[29] I.A. Khan, Y.S. Lee, J.O. Kim, A comparison of variations in blocking mechanisms of membrane-fouling models for estimating flux during water treatment, Chemosphere, 259 (2020) 127328. doi: 10.1016/j.chemosphere.2020.127328
[30] O. Kedem, A. Katchalsky, Permeability of composite membranes Part 1. – electric current, volume flow and flow of solute through membranes, Trans. Faraday Soc., 59 (1963) 1918–1930.
[31] I. Bejaoui, A. Mnif, B. Hamrouni, Influence of operating conditions on the retention of fluoride from water by nanofiltration, Desal. Water Treat., 29 (2011) 39–46.
[32] A.M. Hidalgo, G. León, M. Gómez, M.D. Murcia, E. Gómez, J.L. Gómez, Application of the Spiegler-Kedem-Kachalsky model to the removal of 4-chlorophenol by different nanofiltration membranes, Desalination, 315 (2013) 70–75.
[33] X.L. Wang, T. Tsuru, S.I. Nakao, S. Kimura, The electrostatic and steric-hindrance model for the transport of charged solutes through nanofiltration membranes, J. Membr. Sci., 135 (1997) 19–32.
[34] S.-I. Nakao, S. Kimura, Models of membrane transport phenomena and their applications for ultrafiltration data, J. Chem. Eng. Jpn., 15 (1982) 200–205.
[35] X.-L. Wang, T. Tsuru, M. Togoh, S. Nakao, S. Kimura, Evaluation of pore structure and electrical properties of nanofiltration membranes, J. Chem. Eng. Jpn., 28 (1995) 186–192.
[36] P. Vanýsek, Ionic conductivity and diffusion at infinite dilution, CRC Handb. Chem. Phys., 96 (1996) 5–98.
[37] J. Hermia, Constant pressure blocking filtration laws – application to power-law non-Newtonian fluids, Trans. Inst. Chem. Eng. V, 60 (1982) 183–187.
[38] R.W. Field, D. Wu, J.A. Howell, B.B. Gupta, Critical flux concept for microfiltration fouling, J. Membr. Sci., 100 (1995) 259–272.
[39] C. Jarusutthirak, S. Mattaraj, R. Jiraratananon, Influence of inorganic scalants and natural organic matter on nanofiltration membrane fouling, J. Membr. Sci., 287 (2007) 138–145.
[40] A. Charfi, Etude d'un procédé membranaire de traitement des eaux usées: effet des paramètres biotiques et abiotiques sur le colmatage de la membrane, Universite de Carthage, 2014.
[41] WHO, Water, World Health Organization, 2016. Available at: http://www.who.int/topics/water/en/ (accessed November 23, 2018).
[42] A. Elmidaoui, M.A. Menkouchi Sahli, M. Tahaikt, L. Chay, M. Taky, M. Elmghari, M. Hafsi, Selective nitrate removal by coupling electrodialysis and a bioreactor, Desalination, 153 (2003) 389–397.
[43] A. Fatehizadeh, M.M. Amin, M. Sillanpää, N. Hatami, E. Taheri, N. Baghaei, S. Mahajan, Modeling of fluoride rejection from aqueous solution by nanofiltration process: single and binary solution, Desal. Water Treat., 193 (2020) 224–234.
[44] M. Tahaikt, S. El-Ghzizel, N. Essafi, M. Hafsi, M. Taky, A. Elmidaoui, Technical-economic comparison of nanofiltration and reverse osmosis in the reduction of fluoride ions from groundwater: experimental, modeling, and cost estimate, Desal. Water Treat., 216 (2021) 83–95.
[45] N. Zouhri, M. Igouzal, M. Larif, M. Hafsi, M. Taky, A. Elmidaoui, Prediction of salt rejection by nanofiltration and reverse osmosis membraneusing spiegler-kedem model and an optimisation procedure, Desal. Water Treat., 120 (2018) 41–50.
[46] B. Cuartas-Uribe, M.C. Vincent-Vela, S. Álvarez-Blanco, M.I. Alcaina-Miranda, E. Soriano-Costa, Nanofiltration of sweet whey and prediction of lactose retention as a function of permeate flux using the Kedem-Spiegler and Donnan Steric Partioning models, Sep. Purif. Technol., 56 (2007) 38–46.